Measurement of $\gamma + b + X$ and $\gamma + c + X$ Production Cross Sections in $p \bar{p}$ Collisions at $\sqrt{s} = 1.96$ TeV

V. M. Abazov,[36] B. Abbott,[75] M. Abolins,[65] B. S. Acharya,[29] M. Adams,[51] T. Adams,[49] E. Aguilo,[6] M. Ahsan,[59]
G. D. Alexeev,[36] G. Alkhazov,[40] A. Alton,[64,*] G. Alverson,[63] G. A. Alves,[2] M. Anastasoaie,[35] L. S. Ancu,[35] T. Andeen,[53]
B. Andrieu,[17] M. S. Anzelc,[53] M. Aoki,[50] Y. Arnoud,[14] M. Arov,[60] M. Arthaud,[18] A. Askew,[49,†] B. Åsman,[41]
A. C. S. Assis Jesus,[3] O. Atramentov,[49] C. Avila,[8] J. BackusMayes,[82] F. Badaud,[13] L. Bagby,[50] B. Baldin,[50]
D. V. Bandurin,[59] P. Banerjee,[29] S. Banerjee,[29] E. Barberis,[63] A.-F. Barfuss,[15] P. Bargassa,[80] P. Baringer,[58] J. Barreto,[2]
J. F. Bartlett,[50] U. Bassler,[18] D. Bauer,[43] S. Beale,[6] A. Bean,[58] M. Begalli,[3] M. Begel,[73] C. Belanger-Champagne,[41]
L. Bellantoni,[50] A. Bellavance,[50] J. A. Benitez,[65] S. B. Beri,[27] G. Bernardi,[17] R. Bernhard,[23] I. Bertram,[42] M. Besançon,[18]
R. Beuselinck,[43] V. A. Bezzubov,[39] P. C. Bhat,[50] V. Bhatnagar,[27] G. Blazey,[52] F. Blekman,[43] S. Blessing,[49] K. Bloom,[67]
A. Boehnlein,[50] D. Boline,[62] T. A. Bolton,[59] E. E. Boos,[38] G. Borissov,[42] T. Bose,[77] A. Brandt,[78] R. Brock,[65]
G. Brooijmans,[70] A. Bross,[50] D. Brown,[19] X. B. Bu,[7] N. J. Buchanan,[49] D. Buchholz,[53] M. Buehler,[81] V. Buescher,[22]
V. Bunichev,[38] S. Burdin,[42,‡] T. H. Burnett,[82] C. P. Buszello,[43] P. Calfayan,[25] B. Calpas,[15] S. Calvet,[16] J. Cammin,[71]
M. A. Carrasco-Lizarraga,[33] E. Carrera,[49] W. Carvalho,[3] B. C. K. Casey,[50] H. Castilla-Valdez,[33] S. Chakrabarti,[72]
D. Chakraborty,[52] K. M. Chan,[55] A. Chandra,[48] E. Cheu,[45] D. K. Cho,[62] S. Choi,[32] B. Choudhary,[28] L. Christofek,[77]
T. Christoudias,[43] S. Cihangir,[50] D. Claes,[67] J. Clutter,[58] M. Cooke,[50] W. E. Cooper,[50] M. Corcoran,[80] F. Couderc,[18]
M.-C. Cousinou,[15] S. Crépé-Renaudin,[14] V. Cuplov,[59] D. Cutts,[77] M. Ćwiok,[30] H. da Motta,[2] A. Das,[45] G. Davies,[43]
K. De,[78] S. J. de Jong,[35] E. De La Cruz-Burelo,[33] C. De Oliveira Martins,[3] K. DeVaughan,[67] F. Déliot,[18] M. Demarteau,[50]
R. Demina,[71] D. Denisov,[50] S. P. Denisov,[39] S. Desai,[50] H. T. Diehl,[50] M. Diesburg,[50] A. Dominguez,[67] T. Dorland,[82]
A. Dubey,[28] L. V. Dudko,[38] L. Duflot,[16] S. R. Dugad,[29] D. Duggan,[49] A. Duperrin,[15] S. Dutt,[27] J. Dyer,[65] A. Dyshkant,[52]
M. Eads,[67] D. Edmunds,[65] J. Ellison,[48] V. D. Elvira,[50] Y. Enari,[77] S. Eno,[61] P. Ermolov,[38,§§] M. Escalier,[15] H. Evans,[54]
A. Evdokimov,[73] V. N. Evdokimov,[39] A. V. Ferapontov,[59] T. Ferbel,[61,71] F. Fiedler,[24] F. Filthaut,[35] W. Fisher,[50] H. E. Fisk,[50]
M. Fortner,[52] H. Fox,[42] S. Fu,[50] S. Fuess,[50] T. Gadfort,[70] C. F. Galea,[35] C. Garcia,[71] A. Garcia-Bellido,[71] V. Gavrilov,[37]
P. Gay,[13] W. Geist,[19] W. Geng,[15,65] C. E. Gerber,[51] Y. Gershtein,[49,†] D. Gillberg,[6] G. Ginther,[71] B. Gómez,[8] A. Goussiou,[82]
P. D. Grannis,[72] H. Greenlee,[50] Z. D. Greenwood,[60] E. M. Gregores,[4] G. Grenier,[20] Ph. Gris,[13] J.-F. Grivaz,[16]
A. Grohsjean,[25] S. Grünendahl,[50] M. W. Grünewald,[30] F. Guo,[72] J. Guo,[72] G. Gutierrez,[50] P. Gutierrez,[75] A. Haas,[70]
N. J. Hadley,[61] P. Haefner,[25] S. Hagopian,[49] J. Haley,[68] I. Hall,[65] R. E. Hall,[47] L. Han,[7] K. Harder,[44] A. Harel,[71]
J. M. Hauptman,[57] J. Hays,[43] T. Hebbeker,[21] D. Hedin,[52] J. G. Hegeman,[34] A. P. Heinson,[48] U. Heintz,[62] C. Hensel,[22,§]
K. Herner,[72] G. Hesketh,[63] M. D. Hildreth,[55] R. Hirosky,[81] T. Hoang,[49] J. D. Hobbs,[72] B. Hoeneisen,[12] M. Hohlfeld,[22]
S. Hossain,[75] P. Houben,[34] Y. Hu,[72] Z. Hubacek,[10] N. Huske,[17] V. Hynek,[9] I. Iashvili,[69] R. Illingworth,[50] A. S. Ito,[50]
S. Jabeen,[62] M. Jaffré,[16] S. Jain,[75] K. Johns,[45] C. Johnson,[70] M. Johnson,[50]
D. Johnston,[67] A. Jonckheere,[50] P. Jonsson,[43] A. Juste,[50] E. Kajfasz,[15] D. Karmanov,[38] P. A. Kasper,[50] I. Katsanos,[70]
V. Kaushik,[78] R. Kehoe,[79] S. Kermiche,[15] N. Khalatyan,[50] A. Khanov,[76] A. Kharchilava,[69] Y. N. Kharzheev,[36]
D. Khatidze,[70] T. J. Kim,[31] M. H. Kirby,[53] M. Kirsch,[21] B. Klima,[50] J. M. Kohli,[27] J.-P. Konrath,[23] A. V. Kozelov,[39]
J. Kraus,[65] T. Kuhl,[24] A. Kumar,[69] A. Kupco,[11] T. Kurča,[20] V. A. Kuzmin,[38] J. Kvita,[9] F. Lacroix,[13] D. Lam,[55]
S. Lammers,[70] G. Landsberg,[77] P. Lebrun,[20] W. M. Lee,[50] A. Leflat,[38] J. Lellouch,[17] J. Li,[78,§§] L. Li,[48] Q. Z. Li,[50]
S. M. Lietti,[5] J. K. Lim,[31] J. G. R. Lima,[52] D. Lincoln,[50] J. Linnemann,[65] V. V. Lipaev,[39] R. Lipton,[50] Y. Liu,[7] Z. Liu,[6]
A. Lobodenko,[40] M. Lokajicek,[11] P. Love,[42] H. J. Lubatti,[82] R. Luna-Garcia,[33,||] A. L. Lyon,[50] A. K. A. Maciel,[2]
D. Mackin,[80] R. J. Madaras,[46] P. Mättig,[26] A. Magerkurth,[64] P. K. Mal,[82] H. B. Malbouisson,[3] S. Malik,[67] V. L. Malyshev,[36]
Y. Maravin,[59] B. Martin,[14] R. McCarthy,[72] M. M. Meijer,[35] A. Melnitchouk,[66] L. Mendoza,[8] P. G. Mercadante,[5]
M. Merkin,[38] K. W. Merritt,[50] A. Meyer,[21] J. Meyer,[22,§] J. Mitrevski,[70] R. K. Mommsen,[44] N. K. Mondal,[29] R. W. Moore,[6]
T. Moulik,[58] G. S. Muanza,[15] M. Mulhearn,[70] O. Mundal,[22] L. Mundim,[3] E. Nagy,[15] M. Naimuddin,[50] M. Narain,[77]
H. A. Neal,[64] J. P. Negret,[8] P. Neustroev,[40] H. Nilsen,[23] H. Nogima,[3] S. F. Novaes,[5] T. Nunnemann,[25] D. C. O'Neil,[6]
G. Obrant,[40] C. Ochando,[16] D. Onoprienko,[59] N. Oshima,[50] N. Osman,[43] J. Osta,[55] R. Otec,[10] G. J. Otero y Garzón,[1]
M. Owen,[44] M. Padilla,[48] P. Padley,[80] M. Pangilinan,[77] N. Parashar,[56] S.-J. Park,[22,§] S. K. Park,[31] J. Parsons,[70]
R. Partridge,[77] N. Parua,[54] A. Patwa,[73] G. Pawloski,[80] B. Penning,[23] M. Perfilov,[38] K. Peters,[44] Y. Peters,[26] P. Pétroff,[16]
M. Petteni,[43] R. Piegaia,[1] J. Piper,[65] M.-A. Pleier,[22] P. L. M. Podesta-Lerma,[33,¶] V. M. Podstavkov,[50] Y. Pogorelov,[55]
M.-E. Pol,[2] P. Polozov,[37] B. G. Pope,[65] A. V. Popov,[39] C. Potter,[6] W. L. Prado da Silva,[3] H. B. Prosper,[49] S. Protopopescu,[73]
J. Qian,[64] A. Quadt,[22,§] B. Quinn,[66] A. Rakitine,[42] M. S. Rangel,[2] K. Ranjan,[28] P. N. Ratoff,[42] P. Renkel,[79] P. Rich,[44]

M. Rijssenbeek,[72] I. Ripp-Baudot,[19] F. Rizatdinova,[76] S. Robinson,[43] R. F. Rodrigues,[3] M. Rominsky,[75] C. Royon,[18] P. Rubinov,[50] R. Ruchti,[55] G. Safronov,[37] G. Sajot,[14] A. Sánchez-Hernández,[33] M. P. Sanders,[17] B. Sanghi,[50] G. Savage,[50] L. Sawyer,[60] T. Scanlon,[43] D. Schaile,[25] R. D. Schamberger,[72] Y. Scheglov,[40] H. Schellman,[53] T. Schliephake,[26] S. Schlobohm,[82] C. Schwanenberger,[44] R. Schwienhorst,[65] J. Sekaric,[49] H. Severini,[75] E. Shabalina,[51] M. Shamim,[59] V. Shary,[18] A. A. Shchukin,[39] R. K. Shivpuri,[28] V. Siccardi,[19] V. Simak,[10] V. Sirotenko,[50] P. Skubic,[75] P. Slattery,[71] D. Smirnov,[55] G. R. Snow,[67] J. Snow,[74] S. Snyder,[73] S. Söldner-Rembold,[44] L. Sonnenschein,[17] A. Sopczak,[42] M. Sosebee,[78] K. Soustruznik,[9] B. Spurlock,[78] J. Stark,[14] V. Stolin,[37] D. A. Stoyanova,[39] J. Strandberg,[64] S. Strandberg,[41] M. A. Strang,[69] E. Strauss,[72] M. Strauss,[75] R. Ströhmer,[25] D. Strom,[53] L. Stutte,[50] S. Sumowidagdo,[49] P. Svoisky,[35] A. Sznajder,[3] A. Tanasijczuk,[1] W. Taylor,[6] B. Tiller,[25] F. Tissandier,[13] M. Titov,[18] V. V. Tokmenin,[36] I. Torchiani,[23] D. Tsybychev,[72] B. Tuchming,[18] C. Tully,[68] P. M. Tuts,[70] R. Unalan,[65] L. Uvarov,[40] S. Uvarov,[40] S. Uzunyan,[52] B. Vachon,[6] P. J. van den Berg,[34] R. Van Kooten,[54] W. M. van Leeuwen,[34] N. Varelas,[51] E. W. Varnes,[45] I. A. Vasilyev,[39] P. Verdier,[20] L. S. Vertogradov,[36] M. Verzocchi,[50] D. Vilanova,[18] F. Villeneuve-Seguier,[43] P. Vint,[43] P. Vokac,[10] M. Voutilainen,[67,**] R. Wagner,[68] H. D. Wahl,[49] M. H. L. S. Wang,[50] J. Warchol,[55] G. Watts,[82] M. Wayne,[55] G. Weber,[24] M. Weber,[50,††] L. Welty-Rieger,[54] A. Wenger,[23,‡‡] N. Wermes,[22] M. Wetstein,[61] A. White,[78] D. Wicke,[26] M. R. J. Williams,[42] G. W. Wilson,[58] S. J. Wimpenny,[48] M. Wobisch,[60] D. R. Wood,[63] T. R. Wyatt,[44] Y. Xie,[77] C. Xu,[64] S. Yacoob,[53] R. Yamada,[50] W.-C. Yang,[44] T. Yasuda,[50] Y. A. Yatsunenko,[36] Z. Ye,[50] H. Yin,[7] K. Yip,[73] H. D. Yoo,[77] S. W. Youn,[53] J. Yu,[78] C. Zeitnitz,[26] S. Zelitch,[81] T. Zhao,[82] B. Zhou,[64] J. Zhu,[72] M. Zielinski,[71] D. Zieminska,[54] L. Zivkovic,[70] V. Zutshi,[52] and E. G. Zverev[38]

(The DØ Collaboration)

[1]Universidad de Buenos Aires, Buenos Aires, Argentina
[2]LAFEX, Centro Brasileiro de Pesquisas Físicas, Rio de Janeiro, Brazil
[3]Universidade do Estado do Rio de Janeiro, Rio de Janeiro, Brazil
[4]Universidade Federal do ABC, Santo André, Brazil
[5]Instituto de Física Teórica, Universidade Estadual Paulista, São Paulo, Brazil
[6]University of Alberta, Edmonton, Alberta, Canada,
Simon Fraser University, Burnaby, British Columbia, Canada,
York University, Toronto, Ontario, Canada,
and McGill University, Montreal, Quebec, Canada
[7]University of Science and Technology of China, Hefei, People's Republic of China
[8]Universidad de los Andes, Bogotá, Colombia
[9]Center for Particle Physics, Charles University, Prague, Czech Republic
[10]Czech Technical University, Prague, Czech Republic
[11]Center for Particle Physics, Institute of Physics, Academy of Sciences of the Czech Republic, Prague, Czech Republic
[12]Universidad San Francisco de Quito, Quito, Ecuador
[13]LPC, Université Blaise Pascal, CNRS/IN2P3, Clermont, France
[14]LPSC, Université Joseph Fourier Grenoble 1, CNRS/IN2P3, Institut National Polytechnique de Grenoble, Grenoble, France
[15]CPPM, Aix-Marseille Université, CNRS/IN2P3, Marseille, France
[16]LAL, Université Paris-Sud, IN2P3/CNRS, Orsay, France
[17]LPNHE, IN2P3/CNRS, Universités Paris VI and VII, Paris, France
[18]CEA, Irfu, SPP, Saclay, France
[19]IPHC, Université Louis Pasteur, CNRS/IN2P3, Strasbourg, France
[20]IPNL, Université Lyon 1, CNRS/IN2P3, Villeurbanne, France and Université de Lyon, Lyon, France
[21]III. Physikalisches Institut A, RWTH Aachen University, Aachen, Germany
[22]Physikalisches Institut, Universität Bonn, Bonn, Germany
[23]Physikalisches Institut, Universität Freiburg, Freiburg, Germany
[24]Institut für Physik, Universität Mainz, Mainz, Germany
[25]Ludwig-Maximilians-Universität München, München, Germany
[26]Fachbereich Physik, University of Wuppertal, Wuppertal, Germany
[27]Panjab University, Chandigarh, India
[28]Delhi University, Delhi, India
[29]Tata Institute of Fundamental Research, Mumbai, India
[30]University College Dublin, Dublin, Ireland
[31]Korea Detector Laboratory, Korea University, Seoul, Korea
[32]SungKyunKwan University, Suwon, Korea
[33]CINVESTAV, Mexico City, Mexico

[34]FOM-Institute NIKHEF and University of Amsterdam/NIKHEF, Amsterdam, The Netherlands

[35]Radboud University Nijmegen/NIKHEF, Nijmegen, The Netherlands

[36]Joint Institute for Nuclear Research, Dubna, Russia

[37]Institute for Theoretical and Experimental Physics, Moscow, Russia

[38]Moscow State University, Moscow, Russia

[39]Institute for High Energy Physics, Protvino, Russia

[40]Petersburg Nuclear Physics Institute, Saint Petersburg, Russia

[41]Lund University, Lund, Sweden,
Royal Institute of Technology and Stockholm University, Stockholm, Sweden,
and Uppsala University, Uppsala, Sweden

[42]Lancaster University, Lancaster, United Kingdom

[43]Imperial College, London, United Kingdom

[44]University of Manchester, Manchester, United Kingdom

[45]University of Arizona, Tucson, Arizona 85721, USA

[46]Lawrence Berkeley National Laboratory and University of California, Berkeley, California 94720, USA

[47]California State University, Fresno, California 93740, USA

[48]University of California, Riverside, California 92521, USA

[49]Florida State University, Tallahassee, Florida 32306, USA

[50]Fermi National Accelerator Laboratory, Batavia, Illinois 60510, USA

[51]University of Illinois at Chicago, Chicago, Illinois 60607, USA

[52]Northern Illinois University, DeKalb, Illinois 60115, USA

[53]Northwestern University, Evanston, Illinois 60208, USA

[54]Indiana University, Bloomington, Indiana 47405, USA

[55]University of Notre Dame, Notre Dame, Indiana 46556, USA

[56]Purdue University Calumet, Hammond, Indiana 46323, USA

[57]Iowa State University, Ames, Iowa 50011, USA

[58]University of Kansas, Lawrence, Kansas 66045, USA

[59]Kansas State University, Manhattan, Kansas 66506, USA

[60]Louisiana Tech University, Ruston, Louisiana 71272, USA

[61]University of Maryland, College Park, Maryland 20742, USA

[62]Boston University, Boston, Massachusetts 02215, USA

[63]Northeastern University, Boston, Massachusetts 02115, USA

[64]University of Michigan, Ann Arbor, Michigan 48109, USA

[65]Michigan State University, East Lansing, Michigan 48824, USA

[66]University of Mississippi, University, Mississippi 38677, USA

[67]University of Nebraska, Lincoln, Nebraska 68588, USA

[68]Princeton University, Princeton, New Jersey 08544, USA

[69]State University of New York, Buffalo, New York 14260, USA

[70]Columbia University, New York, New York 10027, USA

[71]University of Rochester, Rochester, New York 14627, USA

[72]State University of New York, Stony Brook, New York 11794, USA

[73]Brookhaven National Laboratory, Upton, New York 11973, USA

[74]Langston University, Langston, Oklahoma 73050, USA

[75]University of Oklahoma, Norman, Oklahoma 73019, USA

[76]Oklahoma State University, Stillwater, Oklahoma 74078, USA

[77]Brown University, Providence, Rhode Island 02912, USA

[78]University of Texas, Arlington, Texas 76019, USA

[79]Southern Methodist University, Dallas, Texas 75275, USA

[80]Rice University, Houston, Texas 77005, USA

[81]University of Virginia, Charlottesville, Virginia 22901, USA

[82]University of Washington, Seattle, Washington 98195, USA

First measurements of the differential cross sections $d^3\sigma/(dp_T^\gamma dy^\gamma dy^{\text{jet}})$ for the inclusive production of a photon in association with a heavy quark (b, c) jet are presented, covering photon transverse momenta $30 < p_T^\gamma < 150$ GeV, photon rapidities $|y^\gamma| < 1.0$, jet rapidities $|y^{\text{jet}}| < 0.8$, and jet transverse momenta $p_T^{\text{jet}} > 15$ GeV. The results are based on an integrated luminosity of 1 fb^{-1} in $p\bar{p}$ collisions at $\sqrt{s} = 1.96$ TeV recorded with the D0 detector at the Fermilab Tevatron Collider. The results are compared with next-to-leading order perturbative QCD predictions.

Photons (γ) produced in association with heavy quarks Q ($\equiv c$ or b) in the final state of hadron-hadron interactions provide valuable information about the parton distributions of the initial state hadrons [1,2]. Such events are produced primarily through the QCD Compton-like scattering process $gQ \rightarrow \gamma Q$, which dominates up to photon transverse momenta (p_T^γ) of ~ 90 GeV for $\gamma + c + X$ and up to ~ 120 GeV for $\gamma + b + X$ production, but also through quark-antiquark annihilation $q\bar{q} \rightarrow \gamma g \rightarrow \gamma Q\bar{Q}$. Consequently, $\gamma + Q + X$ production is sensitive to the b, c, and gluon (g) densities within the colliding hadrons, and can provide constraints on parton distribution functions (PDFs) that have substantial uncertainties [3,4]. The heavy quark and gluon content is an important aspect of QCD dynamics and of the fundamental structure of the proton. In particular, many searches for new physics, e.g., for certain Higgs boson production modes [5–8], will benefit from a more precise knowledge of the heavy quark and gluon content of the proton.

This Letter presents the first measurements of the inclusive differential cross sections $d^3\sigma/(dp_T^\gamma dy^\gamma dy^{\text{jet}})$ for $\gamma + b + X$ and $\gamma + c + X$ production in $p\bar{p}$ collisions, where y^γ and y^{jet} are the photon and jet rapidities [9]. The results are based on an integrated luminosity of 1.02 ± 0.06 fb^{-1} [10] collected with the D0 detector [11] at the Fermilab Tevatron Collider at $\sqrt{s} = 1.96$ TeV. The highest p_T (leading) photon and jet are required to have $|y^\gamma| < 1.0$ and $|y^{\text{jet}}| < 0.8$, and transverse momentum $30 < p_T^\gamma < 150$ GeV and $p_T^{\text{jet}} > 15$ GeV. This selection allows one to probe PDFs in the range of parton-momentum fractions $0.01 \lesssim x \lesssim 0.3$, and hard scatter scales of $9 \times 10^2 \lesssim Q^2 \equiv (p_T^\gamma)^2 \lesssim 2 \times 10^4$ GeV^2. Differential cross sections are presented for two regions of kinematics, defined by $y^\gamma y^{\text{jet}} > 0$ and $y^\gamma y^{\text{jet}} < 0$. These two regions provide greater sensitivity to the parton x because they probe different sets of x_1 and x_2 intervals, as discussed in Ref. [12].

The triggers for this analysis identify clusters of large electromagnetic (EM) energy, and are based on p_T^γ and on the spatial distribution of energy in the photon shower. The trigger efficiency is $\approx 96\%$ for photon candidates with $p_T^\gamma = 30$ GeV and rises to nearly 100% for $p_T^\gamma > 40$ GeV.

To reconstruct photon candidates, towers [11] with large depositions of energy are used as seeds to create clusters of energy in the EM calorimeter in a cone of radius $\mathcal{R} = 0.4$, where $\mathcal{R} \equiv \sqrt{(\Delta\eta)^2 + (\Delta\phi)^2}$ [13]. Once an EM energy cluster is formed, the final energy E_{EM} is defined by a smaller cone of $\mathcal{R} = 0.2$. Photon candidates are required to be isolated within the calorimeter, and must also have $>96\%$ of their energy in its EM section. We require the sum of the total energy inside a cone of $\mathcal{R} = 0.4$, after the subtraction of E_{EM}, to be $<7\%$ of E_{EM}. We also require the width of the energy-weighted shower in the most finely segmented part of the EM calorimeter to be consistent with that expected for an electromagnetic shower, and the probability for any track spatially matched to the photon

EM cluster to be $<0.1\%$. Background from dijet events containing π^0 and η mesons that can mimic photon signatures is also rejected using an artificial neural network for identifying photons (γ-ANN), described in Ref. [12]. The requirement that the γ-ANN output be >0.7, combined with all other photon selection criteria, reduces the dijet event efficiency to 0.1%–0.5%. We calculate photon detection efficiencies using a Monte Carlo (MC) simulation. Signal events are generated using PYTHIA [14] and processed through a GEANT-based [15] simulation of the detector geometry and response, and reconstructed using the same software as for the data. The MC efficiencies are calibrated to those in data using small correction factors measured in $Z \rightarrow e^+ e^-$ samples. The total efficiency of the above photon selection criteria is 63%–80%, depending on p_T^γ. The systematic uncertainties on these values are 5%, and are mainly due to uncertainties in the isolation, the track-match veto, and the γ-ANN requirements.

At least one jet must be present in each event. Jets are reconstructed using the D0 Run II algorithm [16] with a radius of 0.5. The efficiency for a jet to be reconstructed and to satisfy the jet identification criteria is 93%, 96.5%, and 94.5% for light (u, d, s quark or g), c, and b jets at $p_T^\gamma = 30$ GeV and increases to $\approx 98\%$ at $p_T^\gamma = 150$ GeV, independent of the jet flavor. The impact from uncertainties on jet energy scale, jet energy resolution, and difference in energy response between light and $b(c)$ jets is found to be between 8%(6%) and 2%(2%) for p_T^{jet} between 15 GeV and 150 GeV. The leading jet is also required to have at least two associated tracks with $p_T > 0.5$ GeV and the track leading in p_T must have $p_T > 1.0$ GeV, and each track must have at least one hit in the silicon microstrip tracker. The criteria ensure that the jet has sufficient information to be classified as a heavy-flavor (HF) candidate. Light jets are suppressed using a dedicated artificial neural network (b-ANN) [17] that exploits the longer lifetimes of heavy-flavor hadrons relative to their lighter counterparts. The leading jet is required to have a b-ANN output >0.85. Depending on p_T^γ, this selection is 55%–62% efficient for $\gamma + b$ jet, and 11%–12% efficient for $\gamma + c$ jet events, with 3%–5% relative uncertainties on these values. Only 0.2%–1% of light jets are misidentified as heavy-flavor jets.

A primary collision vertex with ≥ 3 tracks is required within 35 cm of the center of the detector along the beam axis. The missing transverse momentum in the event is required to be $<0.7 p_T^\gamma$ so as to suppress background from cosmic-ray muons and $W \rightarrow \ell\nu$ decays. Such a requirement is highly efficient for signal, achieving an efficiency $\geq 96\%$ even for events with semileptonic heavy-flavor quark decays.

About 13 000 events remain in the data sample after applying all selection criteria. Background for photons, stemming mainly from dijet events in which one jet is misidentified as a photon, is still present in this sample.
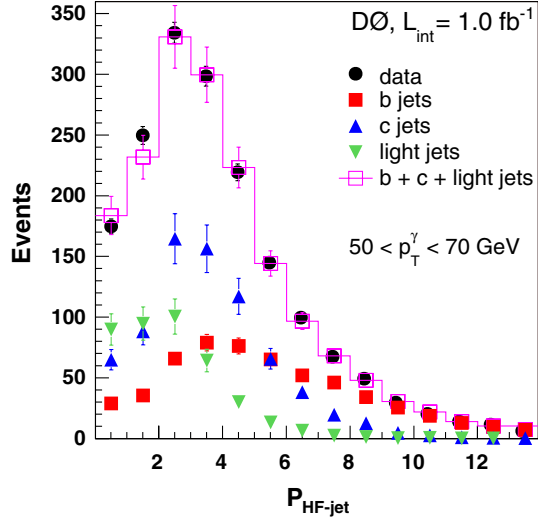
FIG. 1 (color online). Distribution of observed events for P_{HF-jet} after all selection criteria for the bin $50 < p_T^\gamma < 70$ GeV. The distributions for the b, c, and light jet templates are shown normalized to their fitted fraction. Error bars on the templates represent combined uncertainties from statistics of the MC and the fitted jet flavor fractions, while the data contain just statistical uncertainties. Fits in the other p_T^γ bins are of similar quality.

To estimate the photon purity, a template fitting technique is employed [18]. The γ-ANN distribution in data is fitted to a linear combination of templates for photons and jets obtained from simulated γ + jet and dijet samples, respectively. An independent fit is performed in each p_T^γ bin, yielding photon purities between 51% and 93% for $30 < p_T^\gamma < 150$ GeV. The fractional contributions of b and c jets are determined by fitting templates of $P_{HF-jet} = -\ln\prod_i P_{track}^i$ to the data, where P_{track}^i is the probability that a track originates from the primary vertex, based on the significance of the track's distance of closest approach to the primary vertex. All tracks within the jet cone are

used in the fit, except the one with lowest value of P_{track}. Jets from b quarks usually have large values of P_{HF-jet}, whereas light jets mostly have small values, as their tracks originate from the primary vertex. Templates are used for the shape information of the P_{HF-jet} distributions. For b and c jets these are extracted from MC events whereas the light jet template is taken from a data sample enriched in light jets, which is corrected for contributions from b and c quarks. The result of a maximum likelihood fit, normalized to the number of events in data, is shown in Fig. 1 for $50 < p_T^\gamma < 70$ GeV. The estimated fractions of b and c jets in all p_T^γ bins vary between 25%–34% and 40%–48%, respectively. The corresponding uncertainties range between 7%–24%, dominated at higher p_T^γ by the limited data statistics.

The differential cross sections are extracted in five bins of p_T^γ and in the two regions of $y^\gamma y^{jet}$, and are all listed in Table I. The measured cross sections are corrected for the effect of finite calorimeter energy resolution affecting p_T^γ using the unfolding procedure described in Ref. [20]. Such corrections are 1%–3%. The measured differential cross sections are shown in Fig. 2 for $\gamma + b + X$ and $\gamma + c + X$ production as a function of p_T^γ for the jet and photon rapidity intervals in question. The cross sections fall by more than 3 orders of magnitude in the range $30 < p_T^\gamma < 150$ GeV. The statistical uncertainty on the results ranges from 2% in the first p_T^γ bin to $\approx 9\%$ in the last bin, while the total systematic uncertainty varies between 15% and 28%. The main uncertainty at low p_T^γ is due to the photon purity (10.5%) and the heavy-flavor fraction fit (9%). At higher p_T^γ, the uncertainty is dominated by the heavy-flavor fraction. Other significant uncertainties result from the jet-selection efficiency (between 8% and 2%), the photon selection efficiency (5%), and the luminosity (6.1%) [10]. Systematic uncertainties have a 60%–68% correlation between adjacent p_T^γ bins for $30 < p_T^\gamma < 50$ GeV and 20%–30% for $p_T^\gamma > 70$ GeV.

TABLE I. The $\gamma + b + X$ and $\gamma + c + X$ cross sections in bins of p_T^γ in the two regions $y^\gamma y^{jet} > 0$ and $y^\gamma y^{jet} < 0$ together with statistical, $\delta\sigma_{stat}$, and systematic, $\delta\sigma_{syst}$, uncertainties. The theory cross sections σ_{theory} are taken from Ref. [19].

|	p_T^γ bin (GeV)	$\langle p_T^\gamma \rangle$ (GeV)	$y^\gamma y^{jet} > 0$ Cross section (pb/GeV)	$\delta\sigma_{stat}$ (%)	$\delta\sigma_{syst}$ (%)	σ_{theory} (pb/GeV)	$\langle p_T^\gamma \rangle$ (GeV)	$y^\gamma y^{jet} < 0$ Cross section (pb/GeV)	$\delta\sigma_{stat}$ (%)	$\delta\sigma_{syst}$ (%)	σ_{theory} (pb/GeV)
$\gamma + b + X$	30–40	34.1	2.73×10^{-1}	1.5	18.5	2.96×10^{-1}	34.1	2.23×10^{-1}	1.6	19.1	2.45×10^{-1}
	40–50	44.3	1.09×10^{-1}	2.5	15.5	9.31×10^{-2}	44.2	9.53×10^{-2}	2.6	16.0	8.18×10^{-2}
	50–70	57.6	2.72×10^{-2}	3.3	15.2	2.66×10^{-2}	57.4	2.67×10^{-2}	3.3	15.3	2.22×10^{-2}
	70–90	78.7	6.21×10^{-3}	6.6	20.8	6.39×10^{-3}	78.3	6.10×10^{-3}	6.7	20.8	5.49×10^{-3}
	90–150	108.3	1.23×10^{-3}	8.2	26.2	1.11×10^{-3}	110.0	1.09×10^{-3}	8.9	25.7	1.05×10^{-3}
$\gamma + c + X$	30–40	34.1	1.90	1.5	18.1	2.02	34.1	1.56	1.6	18.7	1.59
	40–50	44.3	5.14×10^{-1}	2.5	17.7	5.82×10^{-1}	44.2	4.51×10^{-1}	2.6	18.1	4.56×10^{-1}
	50–70	57.6	1.53×10^{-1}	3.3	17.9	1.41×10^{-1}	57.4	1.50×10^{-1}	3.3	18.0	1.10×10^{-1}
	70–90	78.7	4.45×10^{-2}	6.6	21.3	2.85×10^{-2}	78.3	4.39×10^{-2}	6.7	21.3	2.22×10^{-2}
	90–150	108.3	9.63×10^{-3}	8.2	27.5	3.69×10^{-3}	110.0	8.57×10^{-3}	8.9	27.0	3.28×10^{-3}
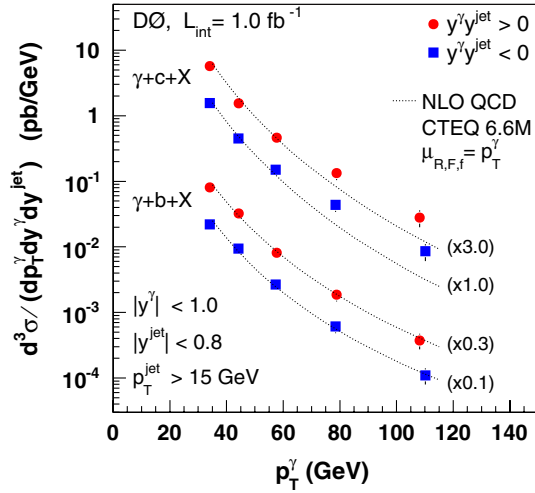
FIG. 2 (color online). The $\gamma + b + X$ and $\gamma + c + X$ differential cross sections as a function of p_T^γ in the two regions $y^\gamma y^{jet} > 0$ and $y^\gamma y^{jet} < 0$. The uncertainties on the data points include statistical and systematic contributions added in quadrature. The NLO pQCD predictions using CTEQ6.6M PDFs are indicated by the dotted lines.
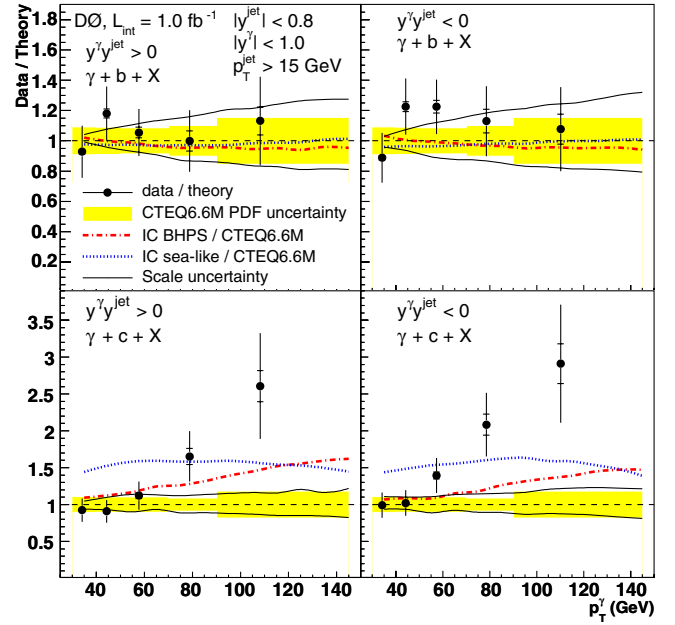

FIG. 3 (color online). The data-to-theory ratio of cross sections as a function of p_T^γ for $\gamma + b + X$ and $\gamma + c + X$ in the regions $y^\gamma y^{jet} > 0$ and $y^\gamma y^{jet} < 0$. The uncertainties on the data include both statistical (inner line) and full uncertainties (entire error bar). Also shown are the uncertainties on the theoretical pQCD scales and the CTEQ6.6M PDFs. The scale uncertainties are shown as dotted lines and the PDF uncertainties by the shaded regions. The ratio of the standard CTEQ6.6M prediction to two models of intrinsic charm is also shown.

Next-to-leading order (NLO) perturbative QCD (pQCD) predictions, with the renormalization scale μ_R, factorization scale μ_F, and fragmentation scale μ_f, all set to p_T^γ, are also given in Table I and compared to data in Fig. 2. These predictions [19] are based on techniques used to calculate the cross section analytically [21], and the ratios of the measured to the predicted cross sections are shown in Fig. 3.

The uncertainty from the choice of the scale is estimated through a simultaneous variation of all three scales by a factor of 2, i.e., to $\mu_{R,F,f} = 0.5p_T^\gamma$ and $2p_T^\gamma$. The predictions utilize CTEQ6.6M PDFs [4], and are corrected for effects of parton-to-hadron fragmentation. This correction for $b(c)$ jets varies from 7.5% (3%) at $30 < p_T^\gamma < 40$ GeV to 1% at $90 < p_T^\gamma < 150$ GeV.

The pQCD prediction agrees with the measured cross sections for $\gamma + b + X$ production over the entire p_T^γ range, and with $\gamma + c + X$ production for $p_T^\gamma < 70$ GeV. For $p_T^\gamma > 70$ GeV, the measured $\gamma + c + X$ cross section is higher than the prediction by about 1.6–2.2 standard deviations (including only the experimental uncertainties) with the difference increasing with growing p_T^γ.

Parametrizations for two models containing intrinsic charm (IC) have been included in CTEQ6.6 [2], and their ratios to the standard CTEQ predictions are also shown in Fig. 3. Both nonperturbative models predict a higher $\gamma + c + X$ cross section. In the case of the BHPS model [2] it grows with p_T^γ. The observed difference may also be caused by an underestimated contribution from the $g \rightarrow Q\bar{Q}$ splitting in the annihilation process that dominates for $p_T^\gamma > 90$ GeV [22].

In conclusion, we have performed the first measurement of the differential cross section of inclusive photon production in association with heavy-flavor (b and c) jets at a $p\bar{p}$ collider. The results cover the range $30 < p_T^\gamma < 150$ GeV, $|y^\gamma| < 1.0$, and $|y^{jet}| < 0.8$. The measured cross sections provide information about b, c, and gluon PDFs for $0.01 \lesssim x \lesssim 0.3$. NLO pQCD predictions using CTEQ6.6M PDFs [19] for $\gamma + b + X$ production agree with the measurements over the entire p_T^γ range. We observe disagreement between theory and data for $\gamma + c + X$ production for $p_T^\gamma > 70$ GeV.

*Visitor from Augustana College, Sioux Falls, South Dakota, USA.

†Visitor from Rutgers University, Piscataway, New Jersey, USA.

‡Visitor from The University of Liverpool, Liverpool, United Kingdom.

§Visitor from II. Physikalisches Institut, Georg-August-University, Göttingen, Germany.

∥Visitor from Centro de Investigacion en Computacion—IPN, Mexico City, Mexico.

¶Visitor from ECFM, Universidad Autonoma de Sinaloa, Culiacán, Mexico.

**Visitor from Helsinki Institute of Physics, Helsinki, Finland.

††Visitor from Universität Bern, Bern, Switzerland.

‡‡Visitor from Universität Zürich, Zürich, Switzerland.

§§Deceased.

[1] B. Bailey, E. L. Berger, and L. E. Gordon, Phys. Rev. D **54**, 1896 (1996).

[2] J. Pumplin, H. L. Lai, and W. K. Tung, Phys. Rev. D **75**, 054029 (2007).

[3] W. K. Tung, arXiv:hep-ph/0409145.

[4] D. Stump et al., J. High Energy Phys. 10 (2003) 046.

[5] S. J. Brodsky, B. Kopeliovich, I. Schmidt, and J. Soffer, Phys. Rev. D **73**, 113005 (2006).

[6] H. J. He and C. P. Yuan, Phys. Rev. Lett. **83**, 28 (1999); C. Balazs, H. J. He, and C. P. Yuan, Phys. Rev. D **60**, 114001 (1999).

[7] K. A. Assamagan, arXiv:hep-ph/0406152.

[8] M. Glück et al., Phys. Lett. B **664**, 133 (2008).

[9] Rapidity is defined as $y = -\ln[(E + p_Z)/(E - p_Z)]$, where E is the energy and p_Z is the momentum component along the proton beam direction.

[10] T. Andeen et al., Report No. FERMILAB-TM-2365, 2007.

[11] V. M. Abazov et al. (D0 Collaboration), Nucl. Instrum. Methods Phys. Res., Sect. A **565**, 463 (2006).

[12] V. M. Abazov et al. (D0 Collaboration), Phys. Lett. B **666**, 435 (2008).

[13] Pseudorapidity η is defined as $\eta = -\ln[\tan(\theta/2)]$, where θ is the polar angle with respect to the proton beam direction, with origin at the center of the detector. ϕ is defined as the azimuthal angle in the plane transverse to the proton beam direction.

[14] T. Sjöstrand et al., Comput. Phys. Commun. **135**, 238 (2001).

[15] R. Brun and F. Carminati, CERN Program Library Long Report No. Writeup W5013, 1993 (unpublished).

[16] G. C. Blazey et al., arXiv:hep-ex/0005012.

[17] T. Scanlon, Ph.D. thesis, FERMILAB THESIS-2006-43.

[18] R. Barlow and C. Beeston, Comput. Phys. Commun. **77**, 219 (1993).

[19] T. Stavreva and J. F. Owens, arXiv:0901.3791v1.

[20] B. Abbott et al. (D0 Collaboration), Phys. Rev. D **64**, 032003 (2001).

[21] B. W. Harris and J. F. Owens, Phys. Rev. D **65**, 094032 (2002).

[22] C. Amsler, Phys. Lett. B **667**, 1 (2008).